Experimental observation of surface states and Landau levels bending in bilayer graphene

Long-Jing Yin, Yu Zhang, Jia-Bin Qiao, Si-Yu Li, and Lin He*

Center for Advanced Quantum Studies, Department of Physics, Beijing Normal University, Beijing 100875, People's Republic of China

(Received 21 October 2015; revised manuscript received 2 March 2016; published 18 March 2016)

We report on microscopic measurements of the low-energy electronic structures both at the zigzag and armchair edges of bilayer graphene using scanning tunneling microscopy and spectroscopy (STM and STS). We have found that, both in the absence and in the presence of a magnetic field, an almost zero-energy peak in the density of states was localized at the zigzag edges, as expected for the surface states at the zigzag edges of bilayer graphene. In the quantum Hall regime, we have clearly observed Landau levels bending away from the charge neutrality point near both the zigzag and armchair edges. Such a result is direct evidence for the evolution of Landau levels into quantum Hall edge states in graphene bilayers. Our experiment indicates that it is possible to explore rich quantum Hall physics in graphene systems using STM and STS.

DOI: 10.1103/PhysRevB.93.125422

There are two possible (perfect) edge terminations, i.e., zigzag and armchair, in graphene monolayers, and the edge orientations strongly affect the electronic structures of graphene sheets [1,2]. Very recently, a graphene system with zigzag edge termination has attracted much attention because its surface states are believed to be closely related to a gap opening [3–6], magnetic order [7], and exceptional ballistic transport [8]. These surface states are dispersionless and do not contribute to the quantum Hall currents. However, in the quantum Hall regime, both the zigzag and armchair edges could bend Landau levels (LLs) to produce dispersive edge states [9–13], which carry the chiral Dirac fermions responsible for the quantum Hall effect (QHE) in graphene monolayers [12,13]. Theoretically, it was predicted that the edges of the monolayer could host crossed dispersive edge states with spin polarization, which are related to symmetry-protected quantum spin Hall phases [10,14]. Transport measurements, however, revealed a strongly insulating behavior with the gapped edges at charge neutrality of monolayer graphene under perpendicular magnetic fields [15,16]. Subsequently, the canted antiferromagnetic edge states, which are due to an edge gap closing by an angled magnetic field, were observed [6], and the expected gapless quantum spin Hall state is believed to be present in a critical value of field [17].

In graphene bilayers, the zigzag edge is also predicted to host surface states at zero fields, but with an enhanced penetration into the bulk compared to that of graphene monolayers [18]. In the presence of high magnetic fields, unconventional QHEs and an abundance of exotic electronic behaviors have been observed [19–26] due to the extra layer degree of freedom, which causes complex edge state configurations in the bilayers. Though much great success has been achieved in the study of the electronic properties of graphene bilayers, considerable work is still necessary to fully understand the nature of the edge states in novel quantum Hall phases. Among the fundamental problems of this system, for example, a direct experimental observation of the surface states at the zigzag edges of a graphene bilayer and its LLs bending at the edge terminations are still lacking. The major challenge may be boiled down to the fabrication of high-quality bilayer samples with the desired edge terminations that are suitable for microscopic investigation. In addition, previous works related to this subject were mainly addressed by optical and transport measurements [27–29], which lack atomic-scale spatial resolution that would be indispensable for studying surface states and LL bending. In this paper, we present scanning tunneling microscopy (STM) and spectroscopy (STS) measurements of bilayer graphene on a graphite substrate both in the absence and in the presence of magnetic fields. The high-quality bilayer sample with atomically sharped edges (Fig. S1) and ultralow random potential fluctuations due to substrate imperfections (Fig. S2) enable us to directly probe the surface states at the zigzag edges and to measure the LLs bending at both the zigzag and armchair edges.

We performed STM measurements in a UNISOKU (USM-1500S) instrument with magnetic fields up to 8 T. The STS spectra, i.e., differential conductance dI/dV curves, were measured with a lock-in detection (modulation voltage 5–10 mV; frequency 793 Hz). The STM tips were obtained by chemical etching from a wire of $Pt_{0.8}Ir_{0.2}$ alloys. The lateral dimensions observed in the STM images were calibrated using a standard graphene lattice and Ag (111) surface. All the STM and STS measurements were performed in an ultrahigh vacuum chamber ($\sim 10^{-11}$ Torr) at $\sim$4.4 K. The bilayer graphene samples used in our experiments were prepared on ZYA grade (from NT-MDT) highly oriented pyrolytic graphite (HOPG) substrates. The HOPG samples were surface cleaved by adhesive tape immediately prior to experiments. The bilayer graphene flakes were deposited on the substrate during the process of mechanical exfoliation and, very importantly, these graphene sheets may decouple from the graphite surface, as demonstrated in previous studies [30–36].

Figure 1(a) shows a representative STM image of a Bernal graphene bilayer on a graphite surface. The triangular contrast in the atomic image arises from the A/B atoms' asymmetry generated by the two adjacent layers. To further identify the bilayer graphene region, we carried out a STS measurement in various magnetic fields, as shown in Fig. 1(b). In zero magnetic field, there are two peaks located at about 0 and 25 mV in the spectrum, which are attributed to the density of states (DOS) peak generated at the valence-band edge (VBE) and

*helin@bnu.edu.cn

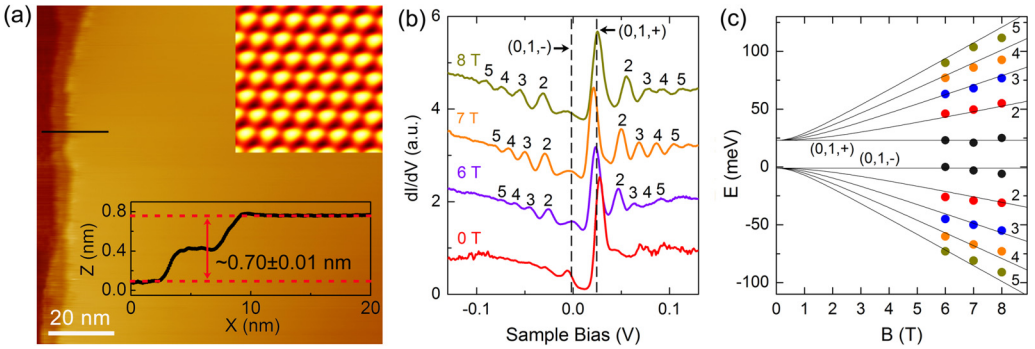

FIG. 1. (a) 100 nm × 100 nm STM topographic image of a bilayer graphene region on a graphite surface ($V_b = 0.2$ V, $I = 0.2$ nA). Inset (upper): Atomic resolution image of the graphene bilayer showing the triangular contrasting, which reflects only one of the two sublattices of the topmost graphene due to the inversion symmetry breaking in Bernal (AB-stacked) bilayers. Inset (lower): Height profile along the black line shows the height difference of two steps $\sim(0.70 \pm 0.01)$ nm, which is slightly larger than the equilibrium spacing of the bilayer step ($\sim$0.67 nm). (b) Tunneling spectra of the graphene bilayers recorded away from the edges under various magnetic fields. LL peak indices are labeled ($+/-$ are valley indices) and the data are offset in the Y axis for clarity. (c) The LL peak energies extracted from (b) plotted vs the magnetic fields B. The solid curves are the fitting of the data with Eq. (1).

conduction-band edge (CBE) of a gapped bilayer, respectively [33,37]. The finite gap in the low-energy bands is generated by inversion symmetry breaking of the adjacent two layers induced by the substrate [33,37–43].

The spectra recorded in high magnetic fields [Fig. 1(b)] exhibit Landau quantization of massive Dirac fermions, as expected for gapped graphene bilayers [20,33,35]. The LL sequences of gapped graphene bilayers can be described by

$$E_n = E_C \pm \{(\hbar\omega_c)^2[n(n-1)] + (U/2)\}^{1/2} - \xi z U/4,$$
$$n = 2,3,4\cdots$$
$$E_0 = E_C + \xi U/2, \quad E_1 = E_C + \xi(U/2)(1-z), \qquad (1)$$

where E_C is the energy of charge neutrality point (CNP), $\omega_c = eB/m^*$ is the cyclotron frequency, m^* is the effective mass of charge carriers, and $\xi = \pm$ are the valley indices. We have $z = 2\hbar\omega_c/t_\perp \ll 1$ for $B \leqslant 8$ T and $|U| \approx E_g$ (gap energy) when the interlayer bias $U < t_\perp$. According to the fitting, as shown in Fig. 1(c), we obtain $E_g \approx 25$ meV and $m^* = (0.035 \pm 0.002)m_e$ (m_e is the free-electron mass). Both the values of E_g and m^* agree well with the previously reported range of values in Bernal bilayers [33,36]. Note that the two lowest levels $\mathrm{LL}_{(0,1,+)}$ and $\mathrm{LL}_{(0,1,-)}$ are a couple of layer-polarized quartets, and they are mainly localized on the first and second graphene layers, respectively. Therefore, the signal of $\mathrm{LL}_{(0,1,+)}$ is much stronger than that of $\mathrm{LL}_{(0,1,-)}$ in the spectra since that the STS predominantly probes the DOS on the top layer.

The measurements demonstrate explicitly that the two topmost layers are Bernal stacked and they are completely decoupled from the substrate. Once a high-quality bilayer graphene region is identified, the structures and electronic properties around its edges are carefully studied. Figures 2(a) and 2(b) show typical atomic-resolution images of a zigzag edge and an armchair edge of the graphene bilayer, respectively. Away from the edges, the STM images exhibit triangular contrasting, as expected to be observed in Bernal bilayers. The types of terminative edges can be determined by the arrangement of the triangular dots, as schematically shown in Figs. 2(a)–2(c). Around both the zigzag and armchair edges, clear interference patterns are observed. Similar interference patterns have also been observed around the edges of a graphene monolayer on a graphite substrate [44–46] and are attributed to the interference between the incident and scattered electron waves in two Dirac cones at the atomically

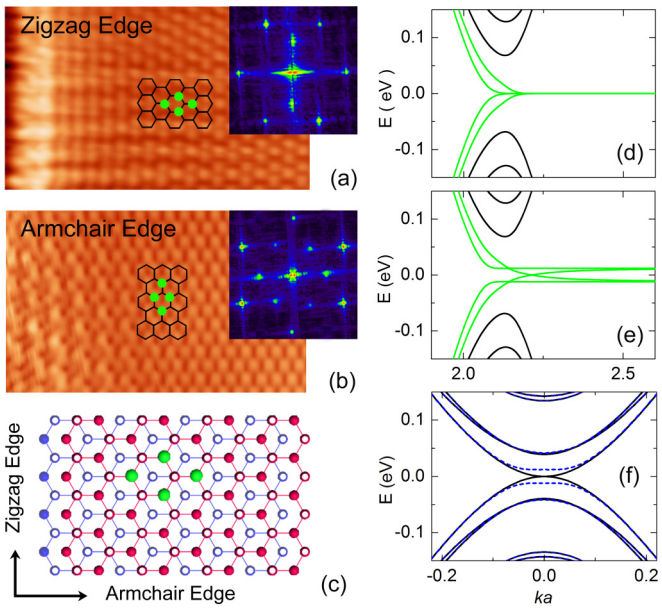

FIG. 2. Atomic resolution images of (a) a zigzag bilayer edge and (b) an armchair bilayer edge. The insets are the the fast Fourier transforms (FFTs) of the STM images. The outer hexangular spots and inner bright spots correspond to the reciprocal lattice of the graphene lattice and the interference of the scattering, respectively. (c) Schematic of the Bernal bilayer graphene with the zigzag and armchair edges. The green dots, representing a set of sublattices imaged in STM topography, can be used to determine the type of graphene edge. Energy spectrum of (d) an unbiased and (e) biased bilayer graphene with zigzag edges. The green curves correspond to the quasilocalized surface states of the two zigzag edges. (f) Energy spectrum of an unbiased (solid curves) and biased (dotted curves) bilayer graphene ribbon with armchair edges.

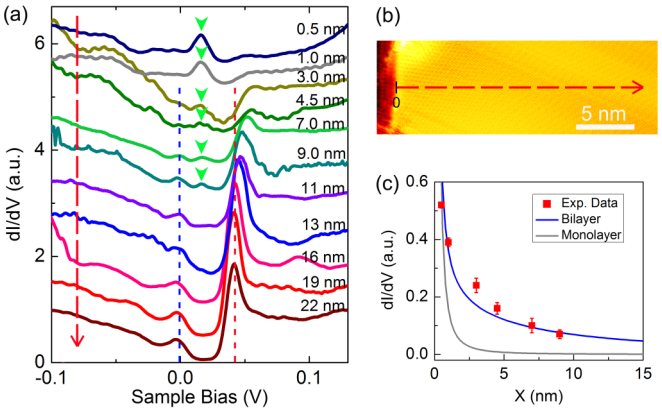

FIG. 3. (a) Spatially resolved STS spectra recorded along the line drawn in (b) around the zigzag edge of bilayer graphene under 0 T. The DOS peaks marked by green arrows correspond to the quasilocalized surface states of the zigzag edge in graphene bilayer. The blue and red dashed lines label the positions of the VBE and the CBE in the bulk graphene bilayer. (c) The decay of the DOS peak height of the surface state obtained in (a). The blue and gray curves correspond to the expected decaying behavior of the surface states in graphene bilayer and monolayer, respectively.

sharped boundaries (see Fig. S1 in the Supplemental Material [47] for more experimental data). The graphene bilayers with zigzag and armchair edges are expected to exhibit quite different electronic band structures: There are localized surface states at the zigzag edges but not at the armchair edges [24,48], as shown in Figs. 2(d)–2(f). In a gapped graphene bilayer with zigzag edges, the surface states may be layer polarized [48] and they are predicted to have a much larger penetration length into the bulk than that in the graphene monolayer [18].

To study the effect of edges on the electronic properties of bilayer graphene, we measured the spatially resolved dI/dV spectra near both the zigzag and armchair edges under zero magnetic field. Figure 3 shows a representative result obtained around a zigzag edge (see Fig. S3 in the Supplemental Material [47] for experimental data recorded around an armchair edge). Typical tunneling spectra recorded at different distances away from the edge are shown in Fig. 3(a) [here we define the zero position at the zigzag edge, as shown in Fig. 3(b)]. When approaching the edge, the signal of the DOS peaks at the VBE and CBE [dashed lines in Fig. 3(a)] becomes weak because the VBE and CBE of a gapped bilayer graphene are exactly valid in the bulk and they are less well defined around the edges. The energy spacing between the VBE and the CBE increases by about 10 meV [Fig. 3(a)], which may arise from a slightly enhanced band gap around the edge. Beside the above-mentioned result, another notable feature of the spectra is the emergence of a new DOS peak around the zigzag edge, and the signal of the peak increases when approaching the edge. Such a peak, which is absent around the armchair edge (Fig. S3), is attributed to a layer-polarized surface state at the zigzag edge of the gapped graphene bilayer [48]. The presence of this DOS peak (surface state) is a fundamental result, and, although it has been anticipated in many theoretical works, it has not been experimentally observed before in graphene bilayers [5,7,8,35,36]. Theoretically, the zigzag surface states are localized at the edge of the bilayers, but its wave function is considerably extended in real space and decays as a function of the distance to the edge. Figure 3(c) plots the measured DOS peak height of the surface state as a function of the distance from the edge. These DOS peaks reflect the local intensity of the surface state wave function. Obviously, the surface state shows a decreasing intensity with increasing distance and extends over 10 nm away from the edge, consistent with the expected decaying behavior of the surface states in graphene bilayers (see the Supplemental Material [47] for details of the calculation). Here we should point out that the decaying length of the surface states in graphene bilayers is much larger than that in graphene monolayers [Fig. 3(c)]. Additionally, the surface state can also be detected even in the quantum Hall regime [Figs. 4(a) and 4(d)].

In two-dimensional electron systems, the low-energy band structures of quasiparticles develop into dispersionless LLs in the presence of a high magnetic field and give rise to the insulating behavior in the bulk, while the confining potential at the edges of the system bends the discrete LLs to form dispersive edge states that carry charge carriers in the quantum Hall effect [10,11,27,28]. The high-quality bilayer sample with crystallographically perfect edges and the ultralow random potential fluctuations induced by the substrate, as demonstrated in Figs. 1–3, allow us to directly probe the LLs bending at the edges.

Figure 4 summarizes the measured result of bilayer graphene in the quantum Hall regime, and we observe clear evidence of LLs bending at both the zigzag and armchair edges (see Fig. S4 in the Supplemental Material [47] for more experimental data). Away from the edges, the well-defined LL spectra, as shown in Figs. 4(a)–4(d), follow the sequence of massive Dirac fermions in gapped graphene bilayers (here we use $l_B = \sqrt{\hbar/eB}$ to define the distance from the edge). When approaching the edges, the DOS peaks for the LLs become weak and the LLs are shifted away from the charge neutrality point, as shown in Figs. 4(e) and 4(f). At a fixed energy, the measured local DOS at position r is determined by the wave functions according to $\rho(r) \propto |\psi(r)|^2$, while the wave functions of LLs have their spatial extent, $\sim 2\sqrt{N} l_B$. It indicates that there is an important contribution from the bulk states even for the recorded LL spectra near the edges. The wave functions of LLs with higher indices have greater spatial extents (see the Supplemental Material [47] for details of the calculation), as shown in the inset of Fig. 4(f). Consequently, the amplitude of high-index LL peaks decreases more slowly than that of low-index LL peaks [Fig. 4(e)], and the bending of low-index LLs seems stronger than that of high-index LLs [Fig. 4(f)] (due to greater contributions from the bulk states to higher LLs).

Theoretically, the shift length of the LLs bending around the edges is predicted to be of magnetic length [10,11]. In Fig. 4(g), we summarize the measured shift length at different magnetic fields around both the zigzag and armchair edges. We find that the shift length depends on neither the magnetic fields nor the edge types, and demonstrate that it is of magnetic length (see Fig. S5 in the Supplemental Material [47] for more experimental data). Additionally, the shift length seems to be dependent on the LL index: The estimated shift lengths

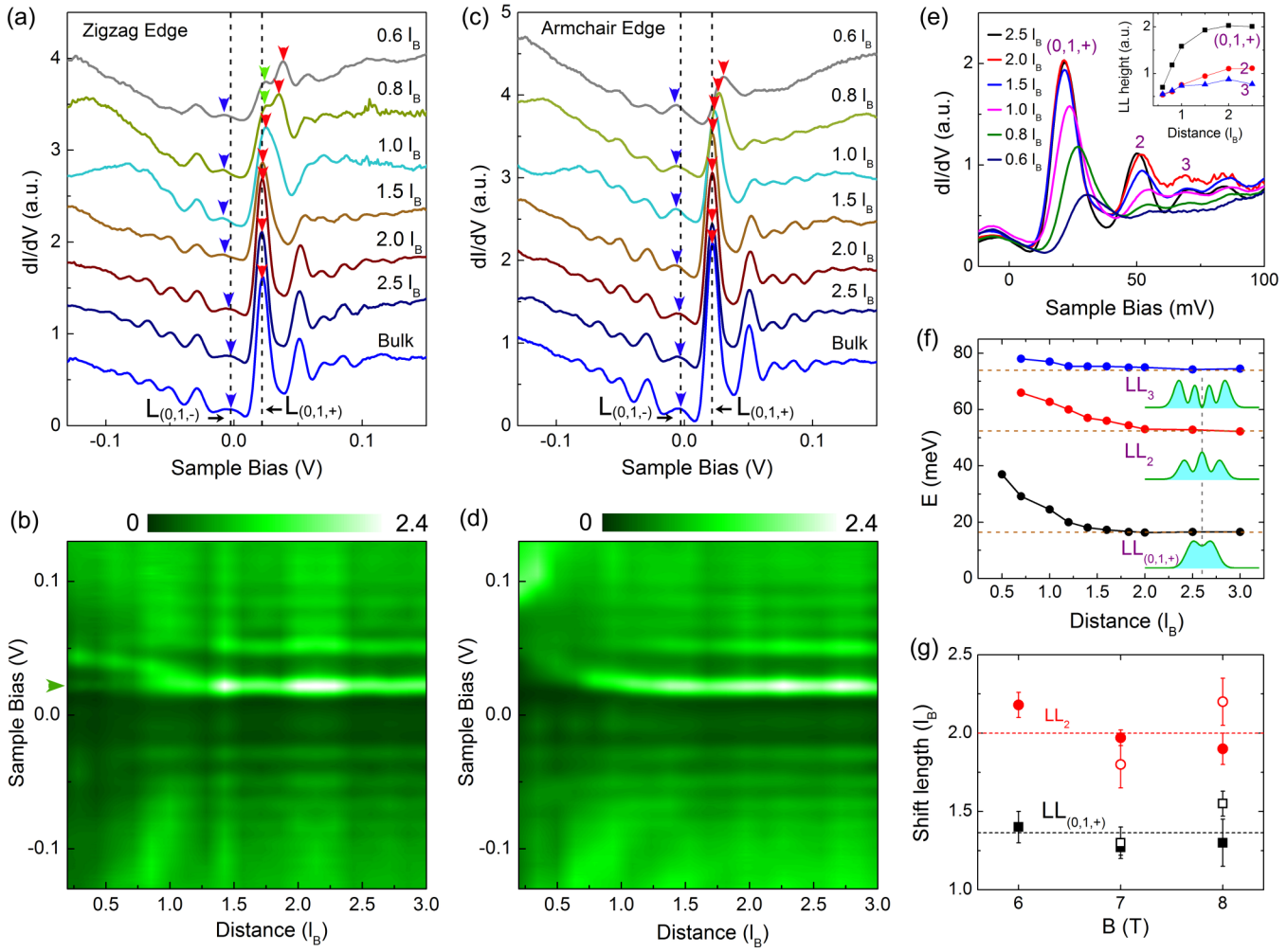

FIG. 4. (a) and (c) show the spatial variation of the LL spectra measured at 7 T around the zigzag and armchair edges of bilayer graphene, respectively. The dashed lines indicate the energy positions of the $LL_{(0,1,-)}$ and $LL_{(0,1,+)}$ in the bulk of bilayer graphene. The blue and red arrows mark the spatial evolution of the $LL_{(0,1,-)}$ and $LL_{(0,1,+)}$ peaks. (b) and (d) show LL spectra maps at 7 T recorded around the zigzag and armchair edges, respectively. In (a) and (b), the peaks marked by green arrows correspond to the quasilocalized surface states of the zigzag edge. (e) Evolution of the peak positions and heights at 7 T with distance from the armchair edge on the conduction-band side. The inset shows LL peak heights extracted from (e) as a function of the distance from the edge. (f) LL bending as a function of distance around the armchair edge measured at 8 T. It shows an explicit shift of the energy positions for the $LL_{(0,1,+)}$, LL_2, and LL_3 toward high energy when approaching the edge. The insets show calculated probability densities for the wave functions of the $LL_{(0,1,+)}$, LL_2, and LL_3 at 8 T. (g) Shift lengths of the $LL_{(0,1,+)}$ and LL_2 bending from the bilayer edges taken at different magnetic fields. The solid dots (open dots) correspond to the data of armchair edges (zigzag edges). The dashed lines are the average values of $\sim 1.4 l_B$ and $\sim 2.0 l_B$ for the $LL_{(0,1,+)}$ and LL_2, respectively.

for the $LL_{(0,1,+)}$ and LL_2 are about $\sim 1.4 l_B$ and $\sim 2.0 l_B$, respectively. Meanwhile, we obtained the average value of the bending energy for the lowest $LL_{(0,1,+)} \sim 65$ meV (see Fig. S6 in the Supplemental Material [47] for more experimental data). This energy scale is approximately identical to the depth of the confining potential well at the sample edge [10,49,50].

In conclusion, we measured the surface state and its spatial evolution around the zigzag edges of bilayer graphene. Our result demonstrates an enhanced penetration length of the surface states in bilayer graphene compared to that in a graphene monolayer. In the quantum Hall regime, we provided direct evidence for the LLs bending around both the zigzag and armchair edges of bilayer graphene, which may open the door to explore exotic quantum Hall physics in graphene bilayers using scanned probe techniques.

This work was supported by the National Basic Research Program of China (Grants No. 2014CB920903 and No. 2013CBA01603), the National Natural Science Foundation of China (Grants No. 11422430 and No. 11374035), the program for New Century Excellent Talents in University of the Ministry of Education of China (Grant No. NCET-13-0054), and Beijing Higher Education Young Elite Teacher Project (Grant No. YETP0238). L.H. also acknowledges support from the National Program for Support of Topnotch Young Professionals.

L.-J.Y. and Y.Z. contributed equally to this work.

[1] A. H. Castro Neto, F. Guinea, N. M. R. Peres, K. S. Novoselov, and A. K. Geim, The electronic properties of graphene, Rev. Mod. Phys. **81**, 109 (2009).

[2] M. O. Goerbig, Electronic properties of graphene in a strong magnetic field, Rev. Mod. Phys. **83**, 1193 (2011).

[3] Y.-W. Son, M. L. Cohen, and S. G. Louie, Half-metallic graphene nanoribbons, Nature (London) **444**, 347 (2006).

[4] M. Han, B. Özyilmaz, Y. Zhang, and P. Kim, Energy Band-Gap Engineering of Graphene Nanoribbons, Phys. Rev. Lett. **98**, 206805 (2007).

[5] Y. Y. Li, M. X. Chen, M. Weinert, and L. Li, Direct experimental determination of onset of electron-electron interactions in gap opening of zigzag graphene nanoribbons, Nat. Commun. **5**, 4311 (2014).

[6] A. F. Young, J. D. Sanchez-Yamagishi, B. Hunt, S. H. Choi, K. Watanabe, T. Taniguchi, R. C. Ashoori, and P. Jarillo-Herrero, Tunable symmetry breaking and helical edge transport in a graphene quantum spin Hall state, Nature (London) **505**, 528 (2014).

[7] G. Z. Magda, X. Jin, I. Hagymasi, P. Vancso, Z. Osvath, P. Nemes-Incze, C. Hwang, L. P. Biro, and L. Tapaszto, Room-temperature magnetic order on zigzag edges of narrow graphene nanoribbons, Nature (London) **514**, 608 (2014).

[8] J. Baringhaus, M. Ruan, F. Edler, A. Tejeda, M. Sicot, A. Taleb-Ibrahimi, A.-P. Li, Z. Jiang, E. H. Conrad, C. Berger, C. Tegenkamp, and W. A. de Heer, Exceptional ballistic transport in epitaxial graphene nanoribbons, Nature (London) **506**, 349 (2014).

[9] V. P. Gusynin and S. G. Sharapov, Unconventional Integer Quantum Hall Effect in Graphene, Phys. Rev. Lett. **95**, 146801 (2005).

[10] D. A. Abanin, P. A. Lee, and L. S. Levitov, Spin-Filtered Edge States and Quantum Hall Effect in Graphene, Phys. Rev. Lett. **96**, 176803 (2006).

[11] G. Li, A. Luican-Mayer, D. Abanin, L. Levitov, and E. Y. Andrei, Evolution of Landau levels into edge states in graphene, Nat. Commun. **4**, 1744 (2013).

[12] K. S. Novoselov, A. K. Geim, S. V. Morozov, D. Jiang, M. I. Katsnelson, I. V. Grigorieva, S. V. Dubonos, and A. A. Firsov, Two-dimensional gas of massless Dirac fermions in graphene, Nature (London) **438**, 197 (2005).

[13] Y. Zhang, Y.-W. Tan, H. L. Stormer, and P. Kim, Experimental observation of quantum Hall effect and Berry's phase in graphene, Nature (London) **438**, 201 (2005).

[14] H. A. Fertig and L. Brey, Luttinger Liquid at the Edge of Undoped Graphene in a Strong Magnetic Field, Phys. Rev. Lett. **97**, 116805 (2006).

[15] J. G. Checkelsky, L. Li, and N. P. Ong, Zero-Energy State in Graphene in a High Magnetic Field, Phys. Rev. Lett. **100**, 206801 (2008).

[16] Z. Jiang, Y. Zhang, H. L. Stormer, and P. Kim, Quantum Hall States Near the Charge-Neutral Dirac Point in Graphene, Phys. Rev. Lett. **99**, 106802 (2007).

[17] M. Kharitonov, Edge excitations of the canted antiferromagnetic phase of the $\nu = 0$ quantum Hall state in graphene: A simplified analysis, Phys. Rev. B **86**, 075450 (2012).

[18] E. V. Castro, N. M. R. Peres, J. M. B. Lopes dos Santos, A. H. Castro Neto, and F. Guinea, Localized States at Zigzag Edges of Bilayer Graphene, Phys. Rev. Lett. **100**, 026802 (2008).

[19] K. S. Novoselov, E. McCann, S. V. Morozov, V. I. Fal'ko, M. I. Katsnelson, U. Zeitler, D. Jiang, F. Schedin, and A. K. Geim, Unconventional quantum Hall effect and Berry's phase of 2π in bilayer graphene, Nat. Phys. **2**, 177 (2006).

[20] E. McCann and V. Fal'ko, Landau-Level Degeneracy and Quantum Hall Effect in a Graphite Bilayer, Phys. Rev. Lett. **96**, 086805 (2006).

[21] F. Zhang and A. H. MacDonald, Distinguishing Spontaneous Quantum Hall States in Bilayer Graphene, Phys. Rev. Lett. **108**, 186804 (2012).

[22] P. Maher, C. R. Dean, A. F. Young, T. Taniguchi, K. Watanabe, K. L. Shepard, J. Hone, and P. Kim, Evidence for a spin phase transition at charge neutrality in bilayer graphene, Nat. Phys. **9**, 154 (2013).

[23] B. J. LeRoy and M. Yankowitz, Emergent complex states in bilayer graphene, Science **345**, 31 (2014).

[24] A. Kou *et al.*, Electron-hole asymmetric integer and fractional quantum Hall effect in bilayer graphene, Science **345**, 55 (2014).

[25] K. Lee *et al.*, Chemical potential and quantum Hall ferromagnetism in bilayer graphene, Science **345**, 58 (2014).

[26] P. Maher *et al.*, Tunable fractional quantum Hall phases in bilayer graphene, Science **345**, 61 (2014).

[27] H. Ito, K. Furuya, Y. Shibata, S. Kashiwaya, M. Yamaguchi, T. Akazaki, H. Tamura, Y. Ootuka, and S. Nomura, Near-Field Optical Mapping of Quantum Hall Edge States, Phys. Rev. Lett. **107**, 256803 (2011).

[28] K. Lai, W. Kundhikanjana, M. A. Kelly, Z.-X. Shen, J. Shabani, and M. Shayegan, Imaging of Coulomb-Driven Quantum Hall Edge States, Phys. Rev. Lett. **107**, 176809 (2011).

[29] J. Tian, Y. Jiang, I. Childres, H. Cao, J. Hu, and Y. P. Chen, Quantum Hall effect in monolayer-bilayer graphene planar junctions, Phys. Rev. B **88**, 125410 (2013).

[30] G. Li, A. Luican, and E. Y. Andrei, Scanning Tunneling Spectroscopy of Graphene on Graphite, Phys. Rev. Lett. **102**, 176804 (2009).

[31] G. Li and E. Y. Andrei, Observation of landau levels of dirac fermions in graphite, Nat. Phys. **3**, 623 (2007).

[32] L.-J. Yin, J. B. Qiao, W. X. Wang, Z. D. Chu, K. F. Zhang, R. F. Dou, C. L. Gao, J. F. Jia, J. C. Nie, and L. He, Tuning structures and electronic spectra of graphene layers with tilt grain boundaries, Phys. Rev. B **89**, 205410 (2014).

[33] L.-J. Yin, S.-Y. Li, J.-B. Qiao, J.-C. Nie, and L. He, Landau quantization in graphene monolayer, Bernal bilayer, and Bernal trilayer on graphite surface, Phys. Rev. B **91**, 115405 (2015).

[34] L.-J. Yin, J.-B. Qiao, W.-J. Zuo, W.-T. Li, and L. He, Experimental evidence for non-Abelian gauge potentials in twisted graphene bilayers, Phys. Rev. B **92**, 081406(R) (2015).

[35] W.-X. Wang, L. J. Yin, J. B. Qiao, T. Cai, S. Y. Li, R. F. Dou, J. C. Nie, X. Wu, and L. He, Atomic resolution imaging of the two-components Dirac Landau levels in graphene monolayer, Phys. Rev. B **92**, 165420 (2015).

[36] G. M. Rutter *et al.*, Microscopic polarization in bilayer graphene, Nat. Phys. **7**, 649 (2011).

[37] E. McCann, Asymmetry gap in the electronic band structure of bilayer graphene, Phys. Rev. B **74**, 161403(R) (2006).

[38] Y. Zhang *et al.*, Direct observation of a widely tunable bandgap in bilayer graphene, Nature (London) **459**, 820 (2009).

[39] E. Castro, K. S. Novoselov, S. V. Morozov, N. M. R. Peres, J. M. B. Lopes dos Santos, J. Nilsson, F. Guinea, A. K. Geim, and

A. H. Castro Neto, Biased Bilayer Graphene: Semiconductor with a Gap Tunable by the Electric Field Effect, Phys. Rev. Lett. **99**, 216802 (2007).

[40] T. Ohta, A. Bostwick, T. Seyller, K. Horn, and E. Rotenberg, Controlling the electronic structure of bilayer graphene, Science **313**, 951 (2006).

[41] K. F. Mak, C. H. Lui, J. Shan, and T. F. Heinz, Observation of an Electric-Field-Induced Band Gap in Bilayer Graphene by Infrared Spectroscopy, Phys. Rev. Lett. **102**, 256405 (2009).

[42] Z. Q. Li, E. A. Henriksen, Z. Jiang, Z. Hao, M. C. Martin, P. Kim, H. L. Stormer, and D. N. Basov, Band Structure Asymmetry of Bilayer Graphene Revealed by Infrared Spectroscopy, Phys. Rev. Lett. **102**, 037403 (2009).

[43] J. B. Oostinga, H. B. Heersche, X. Liu, A. F. Morpurgo, and L. M. Vandersypen, Gate-induced insulating state in bilayer graphene devices, Nat. Mater. **7**, 151 (2008).

[44] Y. Niimi, T. Matsui, H. Kambara, K. Tagami, M. Tsukada, and H. Fukuyama, Scanning tunneling microscopy and spectroscopy of the electronic local density of states of graphite surfaces near monoatomic step edges, Phys. Rev. B **73**, 085421 (2006).

[45] Y. Kobayashi, K.-i. Fukui, and T. Enoki, Edge state on hydrogen-terminated graphite edges investigated by scanning tunneling microscopy, Phys. Rev. B **73**, 125415 (2006).

[46] Y. Kobayashi, K.-i. Fukui, T. Enoki, K. Kusakabe, and Y. Kaburagi, Observation of zigzag and armchair edges of graphite using scanning tunneling microscopy and spectroscopy, Phys. Rev. B **71**, 193406 (2005).

[47] See Supplemental Material at http://link.aps.org/supplemental/10.1103/PhysRevB.93.125422 for more STM images, STS spectra, and details of the analysis.

[48] W. Yao, S. Yang, and Q. Niu, Edge States in Graphene: From Gapped Flat-Band to Gapless Chiral Modes, Phys. Rev. Lett. **102**, 096801 (2009).

[49] D. B. Chklovskii, B. I. Shklovskii, and L. I. Glazman, Electrostatics of edge channels, Phys. Rev. B **46**, 4026 (1992).

[50] L. Brey and H. A. Fertig, Edge states and the quantized Hall effect in graphene, Phys. Rev. B **73**, 195408 (2006).